# Feasibility Analysis and Design of Gas-electricity Integrated Transmission System

Hanchi Zhang, *Member*, *IEEE*, Hongyang Zhou, *Senior Member*, *IEEE*, Filipe Faria da Silva, *Senior Member*, *IEEE*, and Claus Leth Bak, *Senior Member*, *IEEE*

***Abstract*—An increasing number of large-scale renewable plants are generating abundant electricity. As power-to-gas and power-to-x technologies become promising ways to utilize surplus electricity to enhance the flexibility of energy systems, an innovative gas-electricity integrated transmission system (GEITS) to co-transmit electricity and hydrogen or other gas products is proposed, with the foreseeable advantages of compact structure, lower installation cost, and larger energy capacity. This paper investigates the feasibility of GEITS, suggests a design guideline, and gives the operation technical parameters of GEITS in different application scenarios. The dimensions and operating pressures of GEITS benchmark natural gas pipelines and then the nominal voltages of GEITS are calculated based on the electrical strength of high-pressure hydrogen. The nominal ampacities of GEITS are evaluated by temperature-rising simulations, which are larger than those of other transmission lines. Furthermore, high-pressure flowing hydrogen acting as an electrical insulator is a novel topic, and it is investigated via experimental validation on a scale model. Although the effect of 0.4 m/s flowing hydrogen on discharge characteristics has not been observed compared to static hydrogen, the discharge is impaired in 2.4 m/s flowing nitrogen. Future works will investigate the electrical strength of high-pressure long-distance hydrogen gaps under lightning impulse tests and the discharge phenomenon in higher flowing-velocity hydrogen. Methane and methane blended with hydrogen with higher insulation performance can increase the nominal voltages.**

***Index Terms*—Ampacity, gas insulation, high voltage transmission system, hydrogen pipelines, P2X.**

## I. Introduction

LARGE-scale generation of variable renewable electricity (VRE), noticeably wind and solar power, are under development in several countries. Denmark plans to cover 100% of renewable energy demand in some regions [1]. Energy systems are developing towards more flexibility and an increasing proportion of VRE. Power-to-gas (P2G) and power-to-x (P2X) technologies are preferable approaches to utilizing abundant electricity to produce gas fuels and industrial raw materials, such as hydrogen and methane, or convert them into electricity afterward. Meanwhile, the stability and flexibility of the power grid can also be increased.

Generally, the P2G and P2X factories are planned to be close to power plants and substations, far from urban centers and energy-consuming regions [2]. Moreover, the feasibility of offshore grid-integrated P2G is discussed [3], where the P2G facilities are installed beneath the offshore wind turbines. This means that electricity and gases need to be transmitted with a large capacity and over a long distance on close routes. Gases are commonly transmitted by trucks and pipelines [4]. In pipelines, gases are pressed to very high pressures, ranging up to hundreds of bars. Electricity is commonly transmitted by overhead lines (OHLs) and power cables. A few gas-insulated lines (GILs) projects also exist. The electrical design of power cables and GILs are similar: a coaxial structure of central conductors and sheaths insulated by cross-linked polyethylene for the former, or sulfur hexafluoride ($SF_6$) and other more environmental-friendly gaseous insulation that is under investigation for the latter.

All gases are insulated materials, including the hydrogen produced in the electrolyzes of P2G. Thus, there arises a hypothesis: to install an electric conductor in the center of a gas pipe, with the high-pressure, high-velocity gas acting as insulation, to realize the co-transmission of electricity and gas in one structure, namely, Gas-Electricity Integrated Transmission System (GEITS). The demonstration of the concept of GEITS can be seen in Fig. 1.

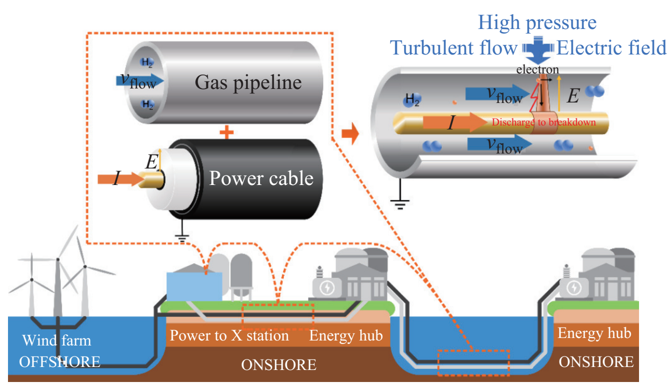


Fig. 1. Demonstrating the "Gas-Electricity Integrated Transmission System" (GEITS) concept.

GEITS can be designed to face different scenarios. For example, low-level GEITS can be used among P2G facilities to energize electrolysis and collect initially produced hydrogen.

Manuscript received August 16, 2024; revised November 1, 2024; accepted January 13, 2025. Date of online publication February 21, 2025; date of current version March 3, 2025.

H. C. Zhang, F. F. da Silva, and C. L. Bak are with the Department of Energy Technology, Aalborg University, Aalborg 9220, Denmark.

H. Y. Zhou (corresponding author, email: eleczhy@163.com) is with the School of Electrical Engineering and Automation, Xiamen University of Technology, Xiamen 361024, China.

DOI: 10.17775/CSEEJPES.2024.06310

GEITS of the medium level can be used to collect hydrogen from all the electrolysis and transmit it to an energy collection hub with electricity. High-level GEITS can be used to transmit large capacities of hydrogen and electricity over long distances. The three levels are collection level, distribution level, and transmission level. GEITS occupies a similar area, and its installation costs are similar to those of a gas pipeline of the same size, but it can fulfil the functions of gas pipelines and power cables. Thus, it can be foreseen to have the advantages of a compact structure, lower installation cost, and larger energy capacity. This paper aims to analyze the feasibility of this novel transmission system through theoretical analysis and experimental validation and to propose preliminary design guidelines for GEITS.

## II. Theoretical Analysis of the Feasibility of Gas-Electricity Integrated Transmission System

The design guideline for GEITS is proposed in this section through theoretical analysis. Firstly, the current hydrogen and natural gas systems are reviewed to benchmark the dimensions and operating pressures of GEITS in different application scenarios. Secondly, the design principle of GILs is reviewed and referred. Thus, the nominal voltages of GEITS are calculated based on the pipelines' sizes and the high-pressure hydrogen's electrical strength. Then, the ampacity and power capacity of GEITS are evaluated based on the heat transfer simulations. Other technical parameters are also calculated based on the electrical design. Additionally, the uniqueness of using high-velocity flowing high-pressure hydrogen as insulation is highlighted, and the relevant research on the effect of airflow discharge phenomena is reviewed to support the theoretical validation of GEITS. The guidelines can be illustrated in Fig. 2 and the detailed procedures in the following subsections.

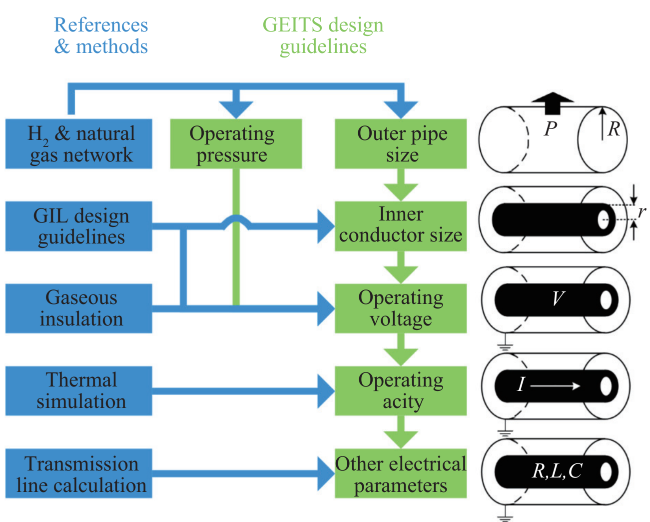


Fig. 2. The flow chart of the design guidelines for GEITS.

### A. Review on the Operation Pressure of Gas Systems

#### 1) Hydrogen Transmission Pressure

Hydrogen transportation mainly uses gaseous-state pipeline transmission, liquid-state pipeline transmission, and traffic transportation. Long-distance transmission pipelines normally operate at high pressures (up to 100 bar). The pipeline diameter in European gas infrastructure ranges from 20 to 48 inches (508 to 1219.2 mm) [5]. Hydrogen transmission pipelines are expected to have a diameter also within this range because the hydrogen infrastructure project in Europe, The European Hydrogen backbone, will use mainly existing infrastructure, which will be properly converted [6]. Some specialized hydrogen transmission pipelines are also under consideration. For example, Danish transmission system operator Energinet has launched a study to determine the feasibility of establishing a west Danish hydrogen transmission grid in Jutland [7]. In the initial phase, the hydrogen pipeline can be operated at lower pressures, e.g., 35/20 bar (inlet pressure/discharge pressure), which can be the discharge pressure from the electrolysis. In the long-term planning, the hydrogen transmission grid is expected to reach 78/30 bar (inlet pressure/outlet pressure) catering to future-proofed large capacity. Out of transport costs, larger pipelines are needed to bring costs down over longer distances. The analyses show that a pipeline dimension of e.g., 36 inches (914 mm) and 78 bar can provide a capacity of 10 GW.

Additionally, it has been investigated whether the existing natural gas infrastructure can be repurposed to a large extent [8]. Therefore, developing an existing natural gas network is also of great value in terms of pipe sizes and operating pressure for benchmarking the application of GEITS.

#### 2) Natural Gas Network Pressure

Natural gas networks are mature in many countries. To meet various demand requirements, the capacity and the pressure of each natural gas pipeline are not constant. There is a general equation to select the high-pressure natural gas pipe size based on the operating parameters, as formulated in (1),

$$D=\frac{Q^{0.381}}{18.93\left(\frac{(P_1^2-P_2^2)\cdot Y}{C_r\cdot L}\right)^{0.206}}\quad \text{(inches)} \tag{1}$$

where $D$ is the inner diameter of the pipe selected, $Q$ is the input volume flow rate in the unit of ft$^3$/h at 60 °F and 30-inch mercury column, $P_1$ and $P_2$ are the inlet pressure and discharge pressure, $L$ is the equivalent length of the pipe whereby the engineer calculates a further length of pipe that will produce an extra friction loss in the pipe that is equivalent to the loss through the fitting. $C_r$ is the viscosity factor which is 0.6094 for natural gas, and $Y$ is the super expansibility factor which is 0.9992 for natural gas. Therefore, the pipe size can be selected in the planning stage by knowing the above parameters.

The natural gas network can be classified into two levels: transmission pipeline systems and distribution pipeline systems. In general, the transmission pipelines have larger diameters and higher operation pressure, which forms the backbone of the natural gas network. Meanwhile, the distribution pipelines to the consumers have relatively lower pressure, larger branches, denser networks and smaller diameters. The pressure-to-size relationship of the natural gas pipelines in different countries is slightly different but generally similar.

Here is a typical example of the natural gas pressure levels in Denmark.

The transmission lines owned and run by Energinet carry natural gas at high pressures of about 40–80 bar. Passing through metering and regulating stations, they are transferred to distribution pipelines run by the distribution system operator at a lower pressure. Through the distribution pipelines, the pressure is further reduced depending on the needs of the consumers; thus, the gas reaches the industrial or household consumers. The technical data for the Danish natural gas network can be found in Table I, which can be benchmarked for the design of GEITS.

TABLE I
TECHNICAL DATA FOR THE DANISH NATURAL GAS NETWORK

| System-level | Transmission level | Distribution level | Street level |
|---|---|---|---|
| Pipe material | Steel | Steel | Plastic |
| Pressure (bar) | 55–164 | 19–50 | 0.022–7 |
| Diameter (mm) | 250–1016 | 80–450 | 40–250 |

### *B. Assessment of Insulation Performance of Electrical Design*

#### *1) Selection and Design of the Insulation Distance: Referring to the Design Principle of GILs*

GEITS has a coaxial electrical structure similar to power cables and GILs. Because power cables use solid polymers as insulation, the aging and thermal factors play an important role in electrical design. The design principle of GILs using gaseous insulation is more informative for designing GEITS. A demonstration of the similar cross-section structure of GILs and GEITS can be seen in Fig. 3, where $r_1$ and $r_2$ are the inner radius and the outer radius of the hollow conductor, $r_3$ and $r_4$ are the inner radius and the outer radius of the enclosure.

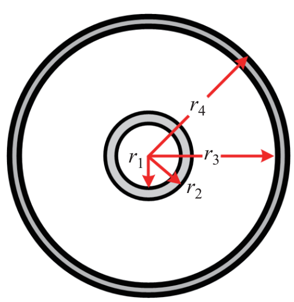


Fig. 3. A demonstration of the cross-section structure of GEITS and GILs.

The dielectric dimensioning of GILs is determined by the maximum allowable electrical field strength, which is identified through voltage tests. The relationship among the maximum allowable electrical field strength $E_m$, the test voltage $V_t$, and the dielectric dimensioning can be described by using Gauss's law as shown in (2) [9],

$$E_m \geq \frac{V_t}{r_2 \ln(r_3/r_2)} \tag{2}$$

For a given outer radius $r_3$, a larger $r_2$ can shorten insulation distances and a smaller $r_2$ can increase the electric field and lower the corona inception voltage on the conductors [10]. Then the dielectric dimensioning is optimized by the best relationship in a cylindrical system where the ratio of $r_3/r_2$ shall be the number "$e$", which makes the derivative of $E_m$ with respect to $r_2$ equal to zero. Thus, (2) can be simplified into (3),

$$E_m \geq \frac{V_t}{r_2} \tag{3}$$

Therefore, to evaluate the dielectric dimensioning $r_2$ for GILs, it is necessary to evaluate $E_m$ and $V_t$.

Firstly, the maximum allowable electrical field strength $E_m$ is evaluated. Generally, $E_m$ is produced according to the 50% breakdown electric field under negative lightning impulse voltage tests $E_{50\%}$. To balance economy and reliability, a design margin is taken into account for GILs as follows,

$$E_m = K_1 E_B \tag{4}$$

$$E_B = E_{50\%}(1 - 3\sigma) \tag{5}$$

Generally, $K_1$ is given 0.85 considering uncertain factors, and $\sigma = 0.05$ is the standard deviation of lightning impulse and switching impulse [11].

Secondly, the test voltages $V_t$ are selected according to the standards. For example, all types of test voltage for 400 kV and 500 kV network GILs can be found in Table II.

TABLE II
TEST VOLTAGE DATA FOR 400 KV AND 500 KV NETWORK GILS

| Test voltage type* | 400 kV network | | 500 kV network | |
|---|---|---|---|---|
| | Factor to $U_m$ | Voltage | Factor to $U_m$ | Voltage |
| $U_N$ | – | 400 kV | – | 500 kV |
| $U_m$ | 1 | 420 kV | 1 | 550 kV |
| $U_{PF}$ | 1.5 | 630 kV | 1.36 | 750 kV |
| $U_{LI}$ | 3.39 | 1425 kV | 2.9 | 1600 kV |
| $U_{SI}$ | 2.5 | 1050 kV | 2.18 | 1200 kV |

*$U_N$: Nominal voltage; $U_m$: Maximum voltage; $U_{PF}$: Power frequency withstand voltage; $U_{LI}$: Lightning impulse voltage; $U_{SI}$: Switching impulse voltage.

Finally, for the dielectric dimensioning of the GIL under a specific nominal voltage, the electric field calculated by (3) with respect to $V_t = U_{LI}$ and $r_2$ shall be smaller than $E_m$. The calculation result of $r_2$ is the inner conductor's minimum allowable radius, and the outer enclosure's corresponding radius can be calculated by timing the optimal ratio "$e$". The above is a general design principle of GILs, and there can be some deviations in practical design for GILs from other considerations and experience.

#### *2) Dielectric Strength of High-pressure Hydrogen*

To design GEITS using high-pressure hydrogen, it is necessary to know the maximum allowable electrical field strength $E_m$, which is evaluated based on the dielectric strength of high-pressure hydrogen. The dielectric strength of gases has been investigated for over one hundred years. Under standard atmospheric conditions (20 °C, 1 atm), hydrogen's uniform breakdown electric field is 17.5 kV/cm while air is about 30 kV/cm [12].

Paschen's law is well-known that the insulation performance of gases in uniform electric field, as quantified by breakdown voltage $V_B$, is related to the product of gas gap distance $d$ and gas pressure $P$ in the following (6),

$$V_B = \frac{B \cdot Pd}{\ln(A \cdot Pd) - \ln[\ln(1 + 1/\gamma_{se})]} \tag{6}$$

where $A$ is the saturation ionization coefficient, $B$ is the excitation and ionization energy coefficient, and $\gamma_{se}$ is the secondary electron emission coefficient, which depends on the electrode material but has limited effect when $Pd$ is large. The values of the constants and the range of application for hydrogen are listed in Table III [13].

TABLE III
PARAMETERS OF HYDROGEN FITTING IN PASCHEN'S LAW

| Parameter | Value |
|---|---|
| $A$ (bar $^{-1}$·cm$^{-1}$) | 3600 |
| $B$ (kV·bar $^{-1}$·cm$^{-1}$) | 102 |
| $\gamma_{se}$ (electrons/ion) [14] | 0.055 |
| Range of $E/p$ (kV·bar $^{-1}$·cm$^{-1}$) | 11.25–450 |

However, based on the application range, it can be reversely deduced that (6) only applies to $Pd$ smaller than 7.11 bar·cm. Other studies on the dielectric strength of hydrogen have been conducted mainly out of pure scientific interest, and short gap distances in uniform electric fields have been tested. The Pd ranges from 30 to 1000 torr·mm, which gives a breakdown voltage of up to 20 kV [15]–[17]. Reference [18] carried out experiments on hydrogen with $Pd$ from 2 to 27 bar·cm (205200 torr·mm), where the breakdown voltage is around 375 kV for Pd of 27 bar·cm. Because hydrogen is rarely used as insulation spacing for practical applications, there is seldom experimental research on the breakdown characteristics of hydrogen under larger $Pd$.

In a non-uniform electric field, corona discharge can occur instead of entire breakdown. The corona discharge of hydrogen as pure physical research has also been studied for years [19]–[21]. In [22], an empirical equation is given to describe the relationship among the corona inception voltage, gas pressure, and the inner conductor radius in a coaxial system within hydrogen, as shown in (7),

$$Pr = 0.0069 \frac{V}{\log_{10}(R/r)} \left( \log_{10} \left( \frac{V}{\log_{10}(R/r)} \right) - 2.61 \right) \tag{7}$$

where $P$ is the gas pressure, $V$ is the voltage on the inner conductor, and $r$ and $R$ are the radii of the inner conductor and the outer enclosure. However, (7) is also summarized based on a small $Pd$ of 3500 torr·mm.

Furthermore, it can be found from the design principle of GILs that the maximum allowable electrical field strength $E_m$ is produced according to the 50% breakdown electric field under negative lightning impulse voltage tests $E_{50\%}$. Lightning impulse voltages are more sensitive to inhomogeneous areas, such as non-uniform electric fields [9]. Impulse breakdown tests on rod-plate electrodes in hydrogen have been carried out in [23], [24], with the pressure in the range of 0.6 bar to 3 bar and spacing up to 25 cm. An empirical equation is proposed to describe the 50 % breakdown voltage of rod-plate electrodes under positive impulse as shown in (8),

$$V_{50\%} = 525 \cdot d^{0.95} \cdot P^{0.7} \quad \text{(kV)} \tag{8}$$

where $d$ is the distance in meters and $P$ is the pressure in bar. It is also argued that, as the breakdown voltage for negative rod-plate is everywhere higher than the positive rod-plate value, the above relation represents the bias for impulse withstand voltage estimation in commercial-purity hydrogen in the present range of pressure and distance [23].

However, it is necessary to mention that the weak point of insulation in gas-insulated systems is the surface of the insulator. There is no research on surface flashover in high-pressure flowing hydrogen, which needs further investigation.

*3) Preliminary Electrical Design of GEITS for Industrial Applications*

The principle of the electrical design of GEITS is also based on (3). For GILs, the dielectric dimensioning is evaluated using the $E_m$ and $V_t$. GEITS must fulfill the requirement to transmit hydrogen simultaneously so that pipe sizes are already given. The principle of the electrical design of GEITS is to evaluate the nominal voltage based on $V_t$ with the given $E_m$ and pipe sizes.

The first step is to select the size of the outer pipe based on the application levels. Then the inner conductor radius can be calculated using the optimal ratio of "$e$". As discussed above, GEITS can be applied at three different levels. Thus, by benchmarking the technical data of natural gas pipelines in Table I, the operating pressures and sizes of GEITS can be selected in Table IV. The sizes of the inner conductors and insulation distances can also be obtained.

TABLE IV
TECHNICAL DATA OF GEITS AT DIFFERENT LEVELS

| System-level | Transmission | Distribution | Collection |
|---|---|---|---|
| Rated pressure (in/out) (bar) | 80/40 | 35/20 | 10/1.5 |
| Pipe diameter $D_2$ (inch/mm) | 40/1016 | 16/406.4 | 10/254 |
| Conductor diameter $D_1$ (mm) | 373.76 | 149.5 | 93.4 |
| Insulation distance $d$ (cm) | 32.10 | 12.85 | 8.00 |

The second step is to estimate the maximum allowable electric field $E_m$. The pressure is selected as the outlet pressure at each application level, where the pressure is the lowest along the whole line. Equation (8) is used to calculate $V_{50\%}$ and $E_{50\%}$ first, then $E_B$ and $E_m$ are calculated by (5) and (4) respectively. The computing results of the maximum allowable electric field $E_m$ are summarized in Table V.

The third step is calculating the maximum test voltage and selecting rated voltage levels according to existing power

TABLE V
RATED VOLTAGE OF GEITS AT DIFFERENT LEVELS

| System-level | Transmission | Distribution | Collection |
|---|---|---|---|
| $V_{50\%}$ (kV) | 2360.69 | 608.61 | 63.29 |
| Max. allowable electric field $E_m$ (kV/cm) | 53.10 | 34.22 | 5.72 |
| Max. lightning test voltage $V_t$ (kV) | 992.33 | 255.79 | 26.69 |
| Lightning impulse voltage $U_{LI}$ (kV) | 950 | 170 | 20 |
| Max. power frequency voltage $U_m$ (kV) | 245 | 36 | 3.6 |
| Nominal voltage $U_N$ (kV) | 220 | 33 | 3.3 |

grids. The maximum standard lightning withstands test voltage $V_t$ can be calculated by (3). According to the IEC std. 60071–1, the rated voltages of GEITS at different levels are selected if they can withstand certain $V_t$ [25]. The rated voltages of GEITS at different levels are also summarized in Table V.

There are several things to be noted. Firstly, it is questionable whether (8) can still be applicable for large $Pd$ in GEITS at the transmission level and the distribution level. Thus, the rated voltage is estimated roughly without rigorous examinations, which needs considerable experimental investigations based on AC withstand tests and lightning/switching impulse withstand tests based on prototypes. Secondly, to fulfill the requirements on the application of a higher rated voltage level, it can be taken into consideration that larger-size pipes and higher pressure are utilized, or other kinds of gases with better insulation ability are adopted.

### C. Calculation of Ampacity Based on Heat Transfer

In all transmission lines, one of the conditions to limit the power transmission capacity, which can be equivalent to the ampacity at the same voltage, is the operating temperature rising that can impact the lifetime of solid materials, such as XLPE in power cables, epoxy spacers in GILs, and the possible insulated supports in GEITS [26]. Heat is mainly produced by the current passing through conductors by Joule's law. Therefore, if more of the heat produced by the current can be dissipated, more current can be carried to the same operating temperature.

GEITS uses hydrogen as insulation material, which has a good heat dissipation ability. Under standard conditions, the thermal conductivity of hydrogen is 0.163 W/(m·K), the highest of all gases. By comparison, the thermal conductivity of air is 0.023 W/(m·K), while the thermal conductivity of the conventional gaseous insulation material $SF_6$ is 0.012 W/(m·K). The pressure-dependent and temperature-dependent thermal conductivities of gases can be found in [27]–[29]. Additionally, heat in gases is not dissipated only by thermal conduction but also by thermal convection. The convective heat transfer coefficient of gases in natural convection is 2–20 W/(m$^2$·K) [30], while the convective heat transfer coefficient of gases in forced convection is 25–300 W/(m$^2$·K) [31]. The hydrogen used in GEITS is transmitted at a high velocity through turbulent flows, enhancing thermal convection and heat dissipation ability.

In the preliminary design, GEITS is expected to carry AC voltage. As a result, it is desirable to design the inner conductor of GEITS as hollow to reduce the usage of aluminum alloy and to increase the capacity of hydrogen because of the skin effect. The skin depth can be calculated in the following (9), which is also the thickness of the hollow conductor in Fig. 3,

$$r_2 - r_1 = \delta = \sqrt{\frac{2\rho}{\omega\mu}} \tag{9}$$

where $\omega$ is the angular frequency, $\rho$ is the resistivity, and $\mu$ is the magnetic permeability. The resistivity and magnetic permeability of aluminum alloy is $2.8 \times 10^{-8}$ Ω·m and $4\pi \times 10^{-7}$ H/m. Thus, the skin depth for 50 Hz AC is 1.19 cm. Generally, when designing GILs' conductors, the thickness of the hollow conductor is 1.27 cm.

Based on the electrical design of GEITS, the thermal distribution of GEITS can be simulated by COMSOL to estimate the ampacity. It is referred to that IEC standard 62271 regulates the temperature limit on the enclosure of GILs [32]. The maximum temperature between 50 °C and 60 °C is considered the applicable limit for direct buried installation. Thus, GEITS installation buried in 15 °C soil is simulated. The maximum ampacity of GEITS at different levels can be calculated and summarized in Table VI.

TABLE VI
RATED VOLTAGE OF GEITS AT DIFFERENT LEVELS

| System-level | Transmission | Distribution | Collection |
|---|---|---|---|
| Nominal voltage $U_N$ (kV) | 220 | 33 | 3.3 |
| Nominal ampacity $I_N$ (A) | 5620 | 3250 | 2430 |
| Transmissible power $P_t$ (MVA) | 2000 | 175 | 13 |

By comparison, the rated ampacity and the transmissible capacity of an example 252 kV GIL is 3150 A and 1300 MVA [33], the rated ampacity and the transmissible capacity of an example 220 kV cable are 1406 A and 500 MVA [34], which are smaller than the rated ampacity of GEITS, because of the better thermal conductivity of hydrogen. However, for GEITS at the distribution and collection levels, although GEITS has a large ampacity, it is still not desirable to carry such a high current because the relatively low voltage results in significant power losses.

### D. Other Electrical Technical Parameters of GEITS

The other electrical technical parameters of GEITS depend on the conductor and outer enclosure dimensions, as shown in Fig. 3.

The resistance per unit length $R_0$ consists of the resistance of the conductor $R_c$ and the enclosure $R_s$, which also depends on the material conductivity $\rho_{c,s}$. $S_c$ and $S_s$ are the cross-section areas of the conductor and the enclosure.

$$R_0 = R_c + R_s \tag{10}$$

$$R_{c,s} = \frac{\rho_{c,s}}{S_{c,s}} \tag{11}$$

$$S_c = \pi(r_2^2 - r_1^2),\ S_s = \pi(r_4^2 - r_3^2) \tag{12}$$

The inductance per unit length $L_0$ and the capacitance per unit length $C_0$ can be calculated by considering the coaxial structure with respect to the magnetic permeability $\mu_0 = 4\pi \times 10^{-7}$ H/m and the permittivity $\varepsilon_0 = 8.854 \times 10^{-12}$ F/m.

$$L_0 = \frac{\mu_0}{2\pi} \ln\frac{r_3}{r_2} \tag{13}$$

$$C_0 = \frac{2\pi\varepsilon_0}{\ln\frac{r_3}{r_2}} \tag{14}$$

Thus, the surge impedance $Z_0$ of GEITS can be calculated in the (15),

$$Z_0 = \frac{1}{2\pi} \ln\frac{r_3}{r_2} \sqrt{\frac{\mu_0}{\varepsilon_0}} \tag{15}$$

To meet the optimal ratio between the enclosure's inner radius and the conductor's outer radius, $r_3/r_2 = e$ is adopted, so $L_0$, $C_0$, and $Z_0$ are constant for varying dimensions of GEITS. The electrical technical parameters of GEITS are summarized in the following Table VII.

TABLE VII
OTHER ELECTRICAL TECHNICAL PARAMETERS OF GEITS AT DIFFERENT LEVELS

| System-level | Transmission | Distribution | Collection |
|---|---|---|---|
| Resistance p.u. $R_0$ (m$\Omega$/km) | 2.05 | 5.40 | 9.12 |
| Inductance p.u. $L_0$ (μH/km) | 200 | 200 | 200 |
| Capacitance p.u. $C_0$ (nF/km) | 55.61 | 55.61 | 55.61 |
| Surge impedance $Z_0$ ($\Omega$) | 59.97 | 59.97 | 59.97 |

The resistance per unit length of GILs is around 6–8 m$\Omega$/km, which is larger than that of GEITS at the transmission level because GEITS has a larger dimension and the conductor cross-section area. Because the capacitance per unit length of GEITS is as low as that of GILs, much lower than that of cables, no or low compensation coils are needed under most network conditions for transmission lengths up to about 100 km [9].

### *E. Review on the Discharge Phenomenon in Flowing Air*

To assess the insulation performance of GEITS, partial discharge is a significant index, which is the early stage of gas insulation breakdown that can lead to power outages and economic losses. However, the case of partial discharge in GEITS is unique because the gas medium where discharge occurs is high-pressure high-velocity flowing hydrogen.

There have been relevant studies on discharge and flashover characteristics in high-velocity air towards the investigation of the roof insulators on the top of high-speed trains. Table VIII lists a review of the research. It can be found that, although the discharge types are different, the results show a higher breakdown voltage under both DC and AC voltage when airflow increases from 0 m/s. However, some also find that the breakdown voltage starts decreasing if the airflow velocity continues increasing. Still, the turning point of airflow velocity varies considerably, for example, 5 m/s in [35], 100 m/s in [36], and 72 m/s in [37], which indicates the turning point of airflow velocity depends a lot on the electric field. DC superposed with impulse voltage is applied in [38] and it is found that the breakdown voltage in the flowing air is lower than that without flowing air. In this case airflow velocity does not increase step by step, so it is questionable whether or where the turning point appears. One exception is in [39] for plate-to-plate electrodes, which shows breakdown voltage slightly decreases with an increasing air flow velocity. It is well explained that there are two mechanisms of airflow affecting discharge phenomena: the airflow blowing effect including the deflection effect and blown away effect, and the airflow density effect [36]. The airflow blowing deflection effect results in the electron path colliding, and the electron number in collision and the concentration of positive ions decrease because of being blown away to weaken discharge and increase breakdown voltage. Meanwhile, higher velocity airflow reduces air density and decreases breakdown voltage. These two effects are dominant in different air velocity ranges.

The above research studied normal pressure air. There has not been any research on the effect of flowing velocity on discharge characteristics in high pressure hydrogen. The discharge processes and mechanisms should be clarified briefly to compare the discharge mechanism between hydrogen and air (nitrogen). The discharge is initialized by electrons colliding with gas molecules. The first Townsend coefficient $\alpha$ describes the number of electrons produced by a single, initiating electron. After that, extra electrons are produced in the secondary process. Two major mechanisms are included in corona discharge: electrons released from the cathode by positive ion bombardment and electrons produced by photoionization when recombination. The secondary Townsend coefficient $\gamma$ represents the number of electrons produced in all secondary mechanisms. During the process, it is accompanied by recombination and attachment, reducing the number of electrons. Recombination coefficient $\beta$ and attachment coefficient $\eta$ are used to describe the reduction of electron numbers in these two mechanisms. Therefore, the above four ionization coefficients must be compared to compare the discharge mechanism between hydrogen and air.

TABLE VIII
LITERATURE REVIEW ON THE DISCHARGE PHENOMENON IN FLOWING AIR

| Scholar & Year | Discharge type | Voltage type | Flow type | Velocity | Effect |
|---|---|---|---|---|---|
| 2009, X. Liu *et al.* [40] | Insulator surface | AC | Orthogonal | 68–136 m/s | Creeping path is blown away |
| 2010, B. He *et al.* [41] | Plate-plate | AC | Orthogonal | 0–15 m/s | $V_b$ increases |
| 2010, W. Sima *et al.* [42] | Surface | AC | | 0–8 m/s | $V_b$ increases |
| 2014, J. Tang *et al.* [35] | Plate-plate | 200 ns Pulse | Orthogonal | 0–5 m/s<br>5–40 m/s | $V_b$ increases<br>$V_b$ decreases |
| 2017, Y. Kang *et al.* [36] | Needle-plate | AC | Orthogonal | 0–100 m/s<br>100–135 m/s | $V_b$ increases<br>$V_b$ slightly decreases |
| 2018, Y. Du *et al.* [43] | Surface | DC | Parallel | 0–90 m/s | Discharge repetition increases.<br>Charge decay rate increases first and decrease. |
| 2018, Y. Kang *et al.* [44] | Needle-needle | DC | Parallel | 82 m/s | Downwind $V_b$ decreases Headwind $V_b$ increases |
| 2018, S. Vogel *et al.* [38] | Needle-plate | +(DC+Imp)<br>−(DC+Imp) | Orthogonal | 22 m/s | No impact<br>$V_b$ decreases |
| 2018, W. Wei *et al.* [45] | Dielectric barrier | AC | Orthogonal | 0–9.7 m/s | No effect on shape, but weaken intensity. |
| 2019, Y. Kang *et al.* [46] | Needle-plate<br>Plate-plate | DC | Orthogonal | 0–120 m/s | $V_b$ increases<br>$V_b$ slightly decreases |
| 2019, D. Zhou *et al.* [47] | Needle-mesh | −DC | Parallel | 0–8.8 m/s | Pulse amplitude decreases first and increases |
| 2021, Y. Du *et al.* [37] | Surface | AC | Parallel | 0–72 m/s<br>72–90 m/s | $V_i$ increases<br>$V_i$ decreases |
| 2021, G. Zhang *et al.* [48] | Insulator surface | DC | Orthogonal | 0–60 m/s | $V_b$ increases |

The four coefficients depend on the electric field, pressure, cathode material ($\gamma_{\rm ion}$), and other conditions. Because the measurement of the coefficients in literature is carried out under various conditions, performing a unified quantitative comparison is difficult. Therefore, a qualitative comparison is performed, as shown below.

The first Townsend coefficient $\alpha$ of hydrogen is higher than that of nitrogen, which means more electrons can be produced initially under the same conditions, or lower energy is needed for hydrogen to produce the same number of electrons [49]. For the measurement of the secondary Townsend coefficient $\gamma$, hydrogen has a lower applicable range of $E/P$ ($E$, the breakdown electric field; $P$, the gas pressure), which is 27–46 V/(cm·torr), than that of nitrogen, which is 54–99 V/(cm·torr). Although at a lower $E$ and the same $P$, positive ion bombardment secondary coefficient $\gamma_{\rm ion}$ of hydrogen is 2–3 times higher than that of nitrogen, while photon secondary coefficient $\gamma_{\rm pho}$ is 5–6 times higher than nitrogen [50], [51] presents that the recombination coefficient $\beta$ at a low nitrogen pressure is about half the value for hydrogen but a rise in the recombination coefficient is noted with increasing pressure. [52] presents that the recombination coefficient $\beta$ at a high nitrogen pressure is two orders of magnitude smaller than that of hydrogen. The recombination process is particularly important at high pressures. For the attachment coefficient $\eta$, both hydrogen and nitrogen are non-attaching gas. However, oxygen is also in the air, and the electrons may be lost by attachment to the neutral molecules to form negative ions [53]. Although the above mechanisms that explain the effect on corona discharge of flowing air can be used as references, it is questionable whether they are still tenable in high-pressure hydrogen, which needs further experimental investigations from the view of the effect on ionization coefficients.

## III. Preliminary Experimental Validation Based on a Scale Model of GEITS

The feasibility of GEITS is analyzed theoretically above, but there remain two aspects for which theoretical analysis is insufficient. One is the insulation strength of a high-pressure long-distance hydrogen gap, while the other is the discharge process in high-pressure high-velocity hydrogen.

Therefore, a scale model is built as a prototype to preliminarily validate the experimental feasibility of GEITS. Corona partial discharge (PD) is the early stage before gaseous insulation breakdown in non-uniform electric field. Thus, the effect on corona development of high-pressure high-flowing-velocity hydrogen can reflect the effect on insulation performance to some extent. This experiment aims to investigate the corona PD characteristics on the surface of the inner conductor in high-pressure flowing hydrogen, to evaluate the insulation performance of the GEITS prototype.

### A. Experimental Setup

#### 1) The Electrical Design of the Test Model of GEITS

The scale model of a coaxial pipe-cable system is designed according to (6). It is designed with a breakdown voltage of 10 kV rms at 1 atm hydrogen. The gas distance is calculated as 9.83 mm. Thus the theoretical radii of the inner conductor and outer pipe are 5.62 mm and 15.28 mm. Considering some margin in case of breakdown, the practical radii of the model used in this research are 6.3 mm and 29.15 mm respectively. The length of the outer pipe is 2 m, while the length of the inner conductor is 1 m which is put in the middle part of the pipe. There are 0.5-m buffering domains inside both ends of the pipe in case of turbulence caused by the input and output of the gas flow. For the inner conductor, one end is supported by a designed insulator, and the other end is suspended by a conducting contact, which is applied to high voltage (HV) from the AC source through a designed "T" shape bushing, as shown in Fig. 4.

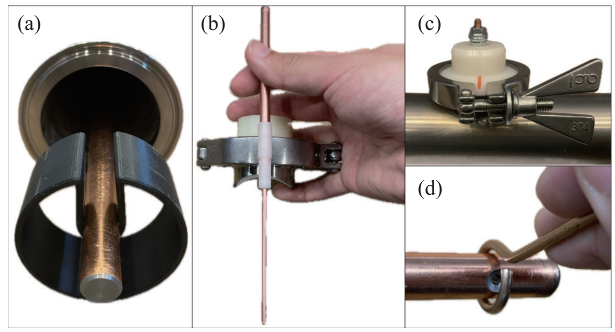


Fig. 4. The configuration of the installation of the inner conductor in the pipe. (a) A designed Teflon insulator to support one end of the central conductor. (b) A conductor to bring HV from outside to inner conductor through a piece of Teflon to keep insulation and gas tightness. (c) "T" shape terminal on the pipe to lead in HV conductor. (d) HV conductor with a hook to suspend the central conductor.

#### 2) The Procedure of the Experiment

An overall configuration of the experimental setup can be seen in Fig. 5 and a graphic demonstration of the experimental setup can be seen in Fig. 6. An HV cable is connected to the conductor to bring the HV potential to the central conductor. The ground wires are screwed with the outer pipe.

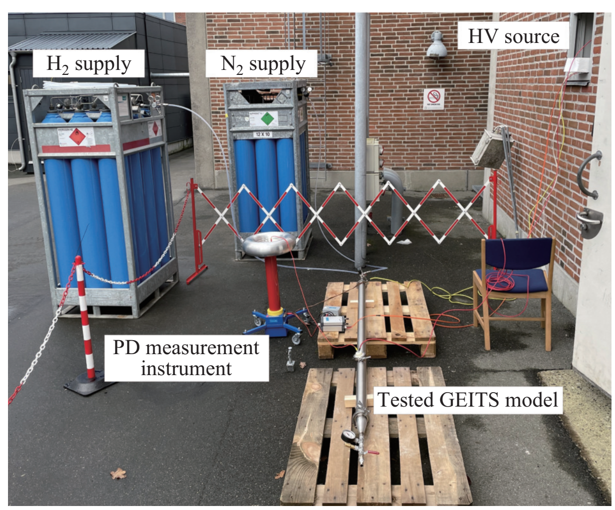


Fig. 5. The overall configuration of the experimental setup of GEITS.

The flammability range of hydrogen is from 4% to 75%, which means if the volume percentage of hydrogen in the air

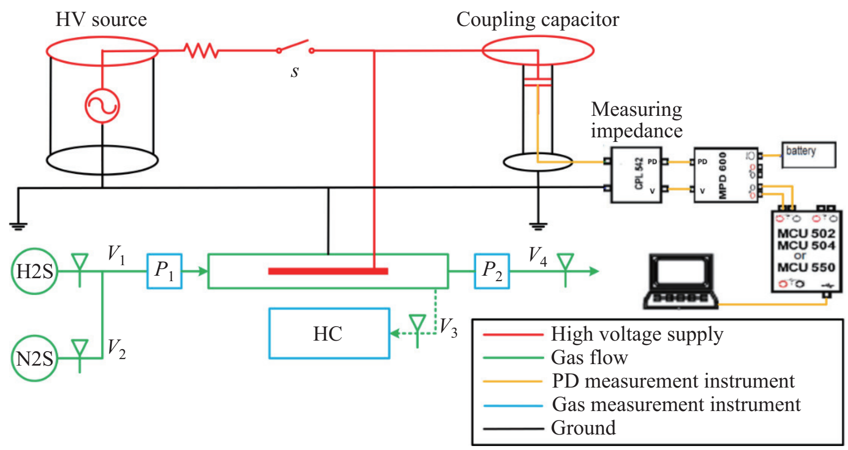


Fig. 6. The demonstration of the experimental setup of GEITS. HC-hydrogen concentration measurement; H2S-hydrogen supply; N2S-nitrogen supply; V-valves; P-pressure gauges.

is within this range, the mixture can be ignited and detonated. In contrast, if the volume percentage of hydrogen in the air is out of this range, the concentration makes hydrogen safe from combustion or explosion [54]. Thus, to guarantee that the concentration of hydrogen is far higher than 75 % and almost no air is mixed with hydrogen, the pipe is flushed with nitrogen before filling in hydrogen. A Y connector parallels together the nitrogen supply bottles and the hydrogen supply bottles. Two regulators are installed to control the outlet's gas pressure and flow rate. PD is detected by Omicron MPD 600.1 using the pulse current method. A high background noise level impacts the outdoor PD test, and the threshold is set as 10 pC to keep the background noise clear.

### *B. Experimental Results*

GEITS prototype is designed with a breakdown voltage of 10 kV rms for 1 atm hydrogen. Based on (8), the breakdown voltage of 3.5 atm hydrogen is 24 kV rms. However, the corona onset voltage and electric field of 3.5 atm hydrogen are 4 kV and 6.35 kV/cm, while the breakdown voltage and electric field are 11 kV and 17.46 kV/cm, much lower than that calculated. This section aims to show the feasibility of applying hydrogen as insulation, and its insulation performance has the potential to be improved by increasing pressure and flowing velocity.

#### *1) Influence of the Hydrogen Flowing Velocity on the Partial Discharge*

The PD characteristics and increasing voltage in static hydrogen are compared with that in the flowing hydrogen. The regulator limits the flow rate at the outlet of hydrogen bottles out of safety. The maximum flow rate is 10 Nm$^3$/h, and the flowing velocity of the hydrogen around the discharge area is calculated as 0.4 m/s at 3.5 atm. The maximum PD magnitude, the average PD magnitude, and the PD repetition in the static hydrogen and flowing hydrogen under 3.5 atm are shown in Figs. 7 and 8 respectively.

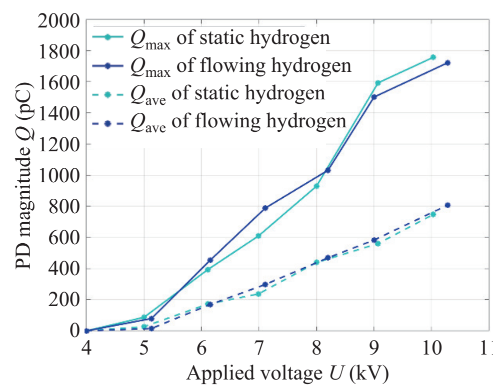


Fig. 7. The maximum PD magnitude and average PD magnitude in the flowing hydrogen compared with those in the static hydrogen under different voltages and 3.5 atm pressure.

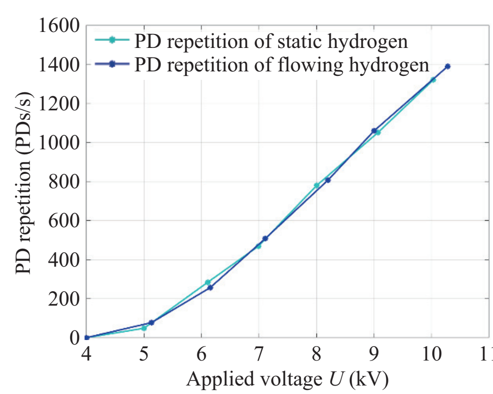


Fig. 8. The PD repetition in the flowing hydrogen compared with those in the static hydrogen under different voltages and 3.5 atm pressure.

In 3.5 atm hydrogen, neither the PD magnitude nor the PD repetition in the flowing hydrogen shows a noticeable difference from those in the static hydrogen. It cannot be concluded that the flowing hydrogen affects the PD dynamics at such a low flow rate (10 Nm$^3$/h) or flowing velocity (0.4 m/s).

#### *2) Supportive Tests on the Comparison of Partial Discharge in Flowing Nitrogen with Static Nitrogen*

Because it cannot be concluded that the flowing hydrogen affects the PD dynamics at such a low flowing velocity (0.4 m/s) limited by the common hydrogen regulator, a higher flowing velocity is achieved using nitrogen with a large-flowing-rate regulator to investigate the effect on the PD. The maximum flow rate limited by the nitrogen regulator is 50 Nm$^3$/h, and the flowing velocity of the nitrogen around the discharge area is calculated as 2.4 m/s at 3 atm. The maximum PD magnitude, the average PD magnitude, and the PD repetition in the static nitrogen and flowing nitrogen under 3 atm are shown in Figs. 9 and 10 respectively.

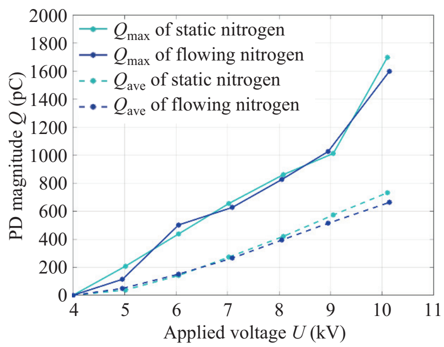


Fig. 9. The maximum PD magnitude and average PD magnitude in the flowing nitrogen compared with those in the static nitrogen under different voltages and 3 atm pressure.

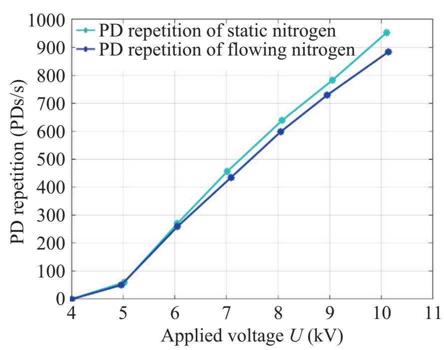


Fig. 10. The PD repetition in the flowing nitrogen compared with that in the static nitrogen under different voltages and 3 atm pressure.

In 3 atm nitrogen, the PD also develops steadily. There is still no obvious difference from the maximum PD magnitude because it has a larger statistical dispersion than the average PD magnitude. However, the average PD magnitude and the PD repetition in the flowing nitrogen have a small reduction, which reach 8 % and 6 % respectively compared with those in the static nitrogen. It can be found that a flowing velocity as high as 2.4 m/s can impair the discharge dynamics to some extent.

## IV. Discussion

### *A. Enhancement on Insulation Performance by Using Blended Hydrogen and Methane*

From Section II-B-2), if the dimension and operating pressure of GEITS at the transmission level benchmark the natural gas transmission pipelines, the rated voltage GEITS as evaluated is limited to 220 kV among the current operating voltage levels. By comparison, power cable lines and GILs are already operating at 500 kV. It can be found from (3), there are two solutions if the allowable voltage is expected to increase.

One is to increase the radius of the inner conductor $r_2$ (the radius of the outer enclosure $r_3$ is also increased at the same time). Larger pipes can be considered for GEITS at the distribution and collection levels. However, GEITS at the transmission level needs more discussion. Firstly, designing pipes with larger diameters and higher pressure requires a larger transmission capacity. However, the largest natural gas transmission pipeline ever designed is the Yamal-Europe pipeline, which installs pipes with a diameter of 56 inches (1420 mm) operating at 100 bar. Thus, if there is no demand for such a large transmission capacity, it is unnecessary to manufacture pipes with larger diameters. Secondly, it is unwise to manufacture larger pipes for longer insulation distances, which increases the hazard level [55], because once leakage or rupture accidents happen, larger pipes with higher pressure under risk assessment can cause more severe consequences.

The other solution is to improve the maximum allowable electric field $E_m$. $E_m$ can be improved by using higher operating pressure, especially the outlet pressure, the lowest part along a pipeline. However, increasing outlet pressure means decreasing the pressure difference between the inlet and outlet, which can decrease the gas flow rate and transmission efficiency. Another plan is to use gas material with higher electrical strength. The idea of GEITS is proposed because of the development of P2G and P2X technologies, which can produce methane based on carbon capture technology. Methane has a better electrical strength than hydrogen [56], [57]. Transmitting methane, or methane blended with hydrogen, can be an alternative for GEITS to carry a higher voltage.

The values of the constants of Paschen's law and the methane application range can be found in [58]. Similarly, the range of application for $Pd$ of methane, which is from 0.0038 bar·cm to 0.03 bar·cm, is even smaller than that of hydrogen. Larger $Pd$ of methane is tested in [59], a 0.1-cm methane gap at 50 bar has a breakdown voltage at around 55 kV. Thus, it is necessary to conduct breakdown tests for $Pd$ in the range applied in GEITS. Moreover, based on the electrical design principle, the maximum allowable electric field is obtained from the 50 % lightning impulse breakdown tests. Thus the lightning impulse tests on non-uniform electric fields with high-pressure methane are also necessary to design GEITS, which have not been investigated before.

Besides, there are still some technical issues with pure hydrogen pipelines, which makes pure hydrogen pipelines not common [60]. There are also material and mechanical issues with hydrogen pipeline transportation that have not been solved, such as hydrogen-related degradation and embrittlement issues [61]. Therefore, methane blended with hydrogen may be more realistic than pure hydrogen because the feasibility of blending hydrogen in natural gas networks has been validated [62].

### *B. Remarks on the Experimental Validation*

Although the experimental validation is preliminary, some remarks must be noted to instruct future work.

During the test, it was found that the breakdown voltage in the hydrogen was lower than that calculated. The reason may be that the breakdown is evaluated based on a perfect coaxial system. Still, the high voltage contact possibly distorts a strong electric field, which incepts PD and leads to breakdown at a lower voltage. The design of how to bring the high voltage to the central conductor must be improved.

The research attempted to investigate the effect of high-velocity-flowing hydrogen on partial discharge, but the flow rate at the outlets of hydrogen bottles was limited. Although the effect of high-velocity gas flow on impairing discharge has been revealed via the tentative experiments using nitrogen, another strategy to inject hydrogen with a high flow rate or flowing velocity should still be proposed and validated.

Another case to be argued is that, during the experiment using flowing nitrogen, because of the absorbing heat when the compressed nitrogen is released, the temperature of the pipe is so low to get frost. Thus, the main reason for the effect of flowing nitrogen on discharge dynamics shall be further distinguished between the flowing velocity and the temperature.

### C. Future Works on the Development of GEITS

Future work shall be conducted in the following areas.

Firstly, the lightning impulse tests and AC breakdown tests shall be conducted on high-pressure long-distance hydrogen. Although (8) is used to evaluate the maximum allowable electric field for hydrogen and it argues that it works with good accuracy in the application range of 0.6–3 bar and 1–25 cm, the pressures and dimensions of GEITS at distribution level and transmission level are far higher than this value. It can be more convincing to evaluate the nominal voltage of GEITS based on the lightning impulse tests on the hydrogen in the same $Pd$ range as tentative applications.

Secondly, the electric strength of methane and methane blended with hydrogen shall be tested. It has been analyzed that it can be a desirable solution to transmit methane and methane blended with hydrogen to obtain a higher nominal voltage. Therefore, the lightning impulse tests shall also be conducted on high-pressure long-distance methane blended with different proportions of hydrogen.

Thirdly, the ampacity of GEITS in other environmental conditions shall be investigated. This paper discussed the ampacity of GEITS buried directly in the soil. There are still possibilities to establish GEITS in open air, underground tunnels, and underwater, which impact heat dissipation and limit ampacity.

Finally, it is necessary to establish an experimental setup that can conduct breakdown and PD tests on high-velocity flowing gases. The high-velocity hydrogen has not been tested in the preliminary experiments. Even though experiments in high-velocity nitrogen showed some impact on the discharge development, the velocity is lower than that in current gas transmission systems. Besides, the impact of temperature also needs to be eliminated.

## V. Conclusion

This paper has investigated the feasibility of a novel gas-electricity integrated transmission system (GEITS), via the theoretical analysis on application scenarios, insulation performance and ampacity, and the experimental validation by a scale model. The following conclusions are summarized.

GEITS can benchmark natural gas pipelines' operating pressure and power grids' rated voltage. Referring to the experience of designing GILs, the principle of designing GEITS has been proposed. The nominal voltages of GEITS can be increased by increasing pipe sizes, increasing outlet pressures, and considering methane/methane blended with hydrogen. The good heat dissipation ability of hydrogen equips GEITS with a large ampacity. At the same nominal voltage, the ampacity of GEITS with hydrogen at transmission level is around 80% higher than that of GILs and over 4 times that of power cables. The literature review shows that flowing air can affect discharge because of airflow blowing and density effects. However, whether they are still tenable in high-pressure hydrogen is questionable which needs further experimental investigations.

Preliminary experimental validation has been conducted to investigate the corona discharge in high-pressure flowing hydrogen. Limited by the hydrogen regulator out of safety, low-velocity-flowing hydrogen does not obviously affect partial discharge. However, the effect of high-velocity gas flow on impairing discharge has been revealed via tentative experiments using nitrogen with a flowing velocity of 2.4 m/s.

The feasibility of GEITS has been investigated in detail. The future work lies in the lightning breakdown tests on the high-pressure long-distance hydrogen gap, better design on testing setup with higher pressure and higher flowing velocity hydrogen, and the attempt on methane and methane blended with hydrogen to reach stronger insulation performance.

## References

[1] J. Z. Thellufsen, H. Lund, P. Sorknæs, P. A. Østergaard, M. Chang, D. Drysdale, S. Nielsen, S. R. Djørup, and K. Sperling, "Smart energy cities in a 100% renewable energy context," *Renewable and Sustainable Energy Reviews*, vol. 129, pp. 109922, Sep. 2020.

[2] T. Estermann, M. Newborough, and M. Sterner, "Power-to-gas systems for absorbing excess solar power in electricity distribution networks," *International Journal of Hydrogen Energy*, vol. 41, no. 32, pp. 13950–13959, Aug. 2016.

[3] North Sea Wind Power Hub, "Grid-integrated offshore Power-to-Gas: a feasibility review and discussion of power grid-integrated offshore Power-to-Gas," North Sea Wind Power Hub, 2022.

[4] E. Abohamzeh, F. Salehi, M. Sheikholeslami, R. Abbassi, and F. Khan, "Review of hydrogen safety during storage, transmission, and applications processes," *Journal of Loss Prevention in the Process Industries*, vol. 72, pp. 104569, Sep. 2021.

[5] A. Wang, K. van der Leun, D. Peters, and M. Buseman, "European hydrogen backbone: how a dedicated hydrogen infrastructure can be created," *Pipeline & Gas Journal*, Jul. 2020.

[6] EHB. The European Hydrogen Backbone (EHB) initiative. [Online]. Available: https://www.ehb.eu/.

[7] Energinet. Feasibility study of hydrogen transmission infrastructure in Jutland. [Online]. Available: https://en.energinet.dk/hydrogen/feasibility-study/.

[8] R. Cardinale, "From natural gas to green hydrogen: developing and repurposing transnational energy infrastructure connecting North Africa to Europe," *Energy Policy*, vol. 181, pp. 113623, Oct. 2023.

[9] H. Koch, *Gas Insulated Transmission Lines (GIL)*. John Wiley & Sons, 2011.

[10] E. Kuffel, W. S. Zaengl, and J. Kuffel, *High Voltage Engineering Fundamentals*. Elsevier Science, 2000.

[11] B. Li, *SF6 High-Voltage Electrical Design*, 5th ed., Beijing: China Machine Press, 2019.

[12] G. R. Astbury and S. J. Hawksworth, “Spontaneous ignition of hydrogen leaks: a review of postulated mechanisms,” *International Journal of Hydrogen Energy*, vol. 32, no. 13, pp. 2178–2185, Sep. 2007.

[13] M. A. Lieberman and A. J. Lichtenberg, “Principles of plasma discharges and materials processing,” *MRS Bulletin*, vol. 30, no. 12, pp. 899–901, Apr. 1994.

[14] E. Jones and F. Llewellyn Jones, “Theory of secondary emission of electrons in hydrogen,” *Proceedings of the Physical Society*, vol. 80, no. 2, pp. 450–464, Aug. 1962.

[15] F. Ehrenkranz, “Spark breakdown potentials as a function of the product of the pressure by the plate separation in A, $N_2$ and $H_2$ for Pt and Na cathodes,” *Physical Review*, vol. 55, no. 2, pp. 219–227, Jan. 1939.

[16] D. H. Hale, “The townsend coefficients for ionization by collision in pure and contaminated hydrogen as a function of the cathode material,” *Physical Review*, vol. 55, no. 9, pp. 815–819, May 1939.

[17] M. J. Druyvesteyn and F. M. Penning, “The mechanism of electrical discharges in gases of low pressure,” *Reviews of Modern Physics*, vol. 12, no. 2, pp. 87–174, Apr. 1940.

[18] E. Finkelmann, “Der elektrische Durchschlag verschiedener Gase unter hohem Druck,” *Archiv für Elektrotechnik*, vol. 31, no. 4, pp. 282–286, Apr. 1937.

[19] J. H. Bruce, “XLV. *Corona discharge in hydrogen*,” *The London, Edinburgh, and Dublin Philosophical Magazine and Journal of Science*, vol. 10, no. 64, pp. 476–480, 1930.

[20] G. L. Weissler, “Positive and negative point-to-plane corona in pure and impure hydrogen, nitrogen, and argon,” *Physical Review*, vol. 63, no. 3–4, pp. 96–107, Feb. 1943.

[21] D. S. Antao, D. A. Staack, A. Fridman, and B. Farouk, “Atmospheric pressure dc corona discharges: operating regimes and potential applications,” *Plasma Sources Science and Technology*, vol. 18, no. 3, pp. 035016, Jun. 2009.

[22] R. O. Jenkins, “The breakdown voltage of cylindrical positive corona discharges in hydrogen,” *International Journal of Electronics*, vol. 23, no. 1, pp. 1–9, Sep. 1967.

[23] O. Farish, S. J. Dale, and A. M. Sletten, “Impulse breakdown of positive rod-plane gaps in hydrogen and hydrogen-SF6 mixtures,” *IEEE Transactions on Power Apparatus and Systems*, vol. 95, no. 5, pp. 1639–1647, Sep. 1976.

[24] O. Farish, S. J. Dale, and A. M. Sletten, “Impulse breakdown of negative rod-plane gaps in hydrogen and hydrogen-SF6 mixtures,” *IEEE Transactions on Power Apparatus and Systems*, vol. PAS-97, no. 1, pp. 118–124, Jan. 1978.

[25] *Insulation Co-Ordination Part 2: Application Guide*, IS/IEC 60071–2: 1996, 2012.

[26] S. Karimi, P. Musilek, and A. M. Knight, “Dynamic thermal rating of transmission lines: a review,” *Renewable and Sustainable Energy Reviews*, vol. 91, pp. 600–612, Aug. 2018.

[27] Y. Tanaka, M. Noguchi, H. Kubota, and T. Makita, “Thermal conductivity of gaseous methane and sulfur hexafluoride under pressure,” *Journal of Chemical Engineering of Japan*, vol. 12, no. 3, pp. 171–176, Jun. 1979.

[28] N. C. Blais and J. B. Mann, “Thermal conductivity of helium and hydrogen at high temperatures,” *The Journal of Chemical Physics*, vol. 32, no. 5, pp. 1459–1465, May 1960.

[29] S. C. Saxena and S. H. P. Chen, “Thermal conductivity of nitrogen in the temperature range 350–2500 K,” *Molecular Physics*, vol. 29, no. 5, pp. 1507–1519, 1975.

[30] C. H. Forsberg, “Chapter 7 - Natural (free) convection,” in *Heat Transfer Principles and Applications*, C. H. Forsberg, Ed. Cambridge: Academic Press, 2021, pp. 267–304.

[31] C. H. Forsberg, “Chapter 6 - Forced convection,” in *Heat Transfer Principles and Applications*, C. H. Forsberg, Ed. Boca Raton: Academic Press, 2021, pp. 211–266.

[32] *High-Voltage Switchgear and Controlgear - Part 203: AC Gas-Insulated Metal-Enclosed Switchgear for Rated Voltages Above 52 kV*, IEC 62271–203: 2022, 2022.

[33] Hitachi Energy. Gas-insulated transmission line (GIL)-high-power transmission up to 6300 A. [Online]. Available: https://www.hitachienergy.com/products-and-solutions/high-voltage-switchgear-and-breakers/gas-insulated-transmission-line.

[34] NKT Cables. High voltage cable systems: cables and accessories up to 550 kV, NKT datasheet. [Online]. Available: https://www.cablejoints.co.uk/upload/NKT_Cables_Extra_High_Voltage_132kV_220kV_400kV_500kV___Brochure.pdf.

[35] J. F. Tang, L. Q. Wei, N. Li, C. S. Ren, and D. R. Yu, “Repetitive nanosecond volume diffuse discharge under airflows,” *IEEE Transactions on Plasma Science*, vol. 42, no. 3, pp. 753–755, Mar. 2014.

[36] Y. Q. Kang, X. Q. Zhang, C. Q. Shi, Y. Zhou, Y. J. Liu, G. Q. Gao, W. F. Wei, and G. N. Wu, “Breakdown characteristics and mechanisms of short needle–plate air gap in high-speed airflow,” *IEEE Transactions on Plasma Science*, vol. 45, no. 9, pp. 2406–2415, Sep. 2017.

[37] Y. Du, Q. D. Zhu, C. Li, J. Zhang, D. Liu, and M. Zhao, “Influence of gas flow on surface discharge development under AC voltage,” in *22nd International Symposium on High Voltage Engineering (ISH 2021)*, Xi’an, China, 2021, pp. 2152–2155.

[38] S. Vogel and J. Holboll, “Experimental evaluation of discharge characteristics in inhomogeneous fields under air flow,” *IEEE Transactions on Dielectrics and Electrical Insulation*, vol. 25, no. 2, pp. 721–728, Apr. 2018.

[39] Y. Q. Kang, G. N. Wu, X. Q. Zhang, Y. J. Liu, C. Q. Shi, W. F. Wei, and G. Q. Gao, “Modeling of flowing gas discharge – Part I,” *IEEE Transactions on Dielectrics and Electrical Insulation*, vol. 26, no. 4, pp. 1048–1055, Aug. 2019.

[40] X. Z. Liu, C. Gao, X. B. Deng, L. Q. Cao, and X. C. Chen, “The influence of high-velocity airflow on discharge characteristics of electric locomotive roof insulator,” in *2009 IEEE 9th International Conference on the Properties and Applications of Dielectric Materials*, Harbin, China, 2009, pp. 453–456.

[41] B. He, G. Zhang, B. F. Chen, N. K. Gao, Y. Z. Li, Z. R. Peng, and H. Y. Jin, “The influence of the sand-dust environment on air-gap breakdown discharge characteristics of the plate-to-plate electrode,” *Science China Physics, Mechanics and Astronomy*, vol. 53, no. 3, pp. 458–464, Mar. 2010.

[42] W. X. Sima, Q. Yang, G. Q. Ma, C. L. Jiang, L. Wu, and H. Cheng, “Experiments and analysis of sand dust flashover of the flat plate model,” *IEEE Transactions on Dielectrics and Electrical Insulation*, vol. 17, no. 2, pp. 572–581, Apr. 2010.

[43] Y. Du, Y. P. Meng, K. Wu, X. Z. Ma, W. J. Song, and X. Yang, “Influence of gas flow on surface charge decay of partial discharge under DC voltage,” in *2018 12th International Conference on the Properties and Applications of Dielectric Materials (ICPADM)*, Xi’an, China, 2018, pp. 132–135.

[44] Y. Q. Kang, G. N. Wu, X. Q. Zhang, Y. J. Guo, C. Q. Shi, and Y. J. Liu, “Polarity effect of flowing air discharge,” *IEEE Access*, vol. 6, pp. 61819–61825, Oct. 2018.

[45] W. F. Wei, S. He, S. Wang, X. Yan, and G. Q. Gao, “Effects of airflow on atmospheric pressure surface dielectric barrier discharge,” in *2018 IEEE International Conference on High Voltage Engineering and Application (ICHVE)*, Athens, Greece, 2018, pp. 1–4.

[46] Y. Q. Kang, G. N. Wu, X. Q. Zhang, Y. J. Liu, C. Q. Shi, W. F. Wei, and G. Q. Gao, “Verification and analysis of flowing gas discharge – Part II,” *IEEE Transactions on Dielectrics and Electrical Insulation*, vol. 26, no. 4, pp. 1056–1064, Aug. 2019.

[47] D. S. Zhou, J. F. Tang, M. Tang, X. M. Zhu, and C. H. Zhang, “Nonmonotonous phenomenon of corona discharge characteristics under different airflow rates,” *IEEE Transactions on Plasma Science*, vol. 47, no. 5, pp. 1964–1970, May 2019.

[48] G. Q. Zhang, X. Q. Zhang, Y. J. Guo, B. Wang, F. Yang, and G. N. Wu, “Study on characteristics of surface discharge of silicone rubber under high-speed airflow,” in *2021 IEEE Electrical Insulation Conference (EIC)*, Denver, CO, USA, 2021, pp. 359–362.

[49] D. J. DeBitetto and L. H. Fisher, “Townsend ionization coefficients and uniform field breakdown in hydrogen and nitrogen at high pressures,” *Physical Review*, vol. 104, no. 5, pp. 1213–1220, Dec. 1956.

[50] H. Tagashira and J. Lucas, “The measurement of ionization coefficients in hydrogen and nitrogen,” *Journal of Physics D: Applied Physics*, vol. 2, no. 6, pp. 867–880, 1969.

[51] M. A. Biondi and S. C. Brown, “Measurement of electron-ion recombination,” *Physical Review*, vol. 76, no. 11, pp. 1697–1700, Dec. 1949.

[52] D. R. Bates, V. Malaviya, and N. A. Young, “Electron-ion recombination in a dense molecular gas,” *Proceedings of the Royal Society of London. A. Mathematical and Physical Sciences*, vol. 320, no. 1543, pp. 437–458, Jan. 1971.

[53] R. Hackam, “Total secondary ionization coefficients and breakdown potentials of hydrogen, methane, ethylene, carbon monoxide, nitrogen, oxygen and carbon dioxide between mild steel coaxial cylinders,” *Journal of Physics B: Atomic and Molecular Physics*, vol. 2, no. 2, pp. 216–233, 1969.

[54] D. Bjerketvedt, J. R. Bakke, and K. van Wingerden, “Gas explosion handbook,” *Journal of Hazardous Materials*, vol. 52, no. 1, pp. 1–150, Jan. 1997.

[55] A. G. Shiryaev, S. G. Chetverikov, S. G. Chikalov, I. Y. Pyshmintsev, and P. V. Krylov, “Production of seamless steel pipe for oil and gas extraction

in challenging conditions," *Steel in Translation*, vol. 48, no. 11, pp. 704–711, 2018.
[56] E. Sagnes, J. Szurmak, D. Manage, and S. Zukotynski, "Study of the dc saddle-field discharge: application to methane," *Journal of Vacuum Science & Technology A*, vol. 17, no. 3, pp. 713–720, May 1999.
[57] P. Bletzinger, "Determination of breakdown voltages and instabilities in electron beam ionized discharges," Air Force Wright Aeronautical Laboratories Wright-Patterson AFB, Ohio, OMB No. 0704–0188, 1985.
[58] A. E. D. Heylen, "Influence of molecular bonding on the Townsend ionization coefficients of hydrocarbon gases," *The Journal of Chemical Physics*, vol. 38, no. 3, pp. 765–771, Feb. 1963.
[59] B. W. Ward and T. J. Lewis, "The electric strength and conduction of methane gas at high pressures," in *Annual Report 1963 Conference on Electrical Insulation*, White Sulphur Springs, WV, USA, 1963, pp. 103–106.
[60] M. Ball and M. Wietschel, "The future of hydrogen–opportunities and challenges," *International Journal of Hydrogen Energy*, vol. 34, no. 2, pp. 615–627, Jan. 2009.
[61] E. Ohaeri, U. Eduok, and J. Szpunar, "Hydrogen related degradation in pipeline steel: a review," *International Journal of Hydrogen Energy*, vol. 43, no. 31, pp. 14584–14617, Aug. 2018.
[62] J. B. Cristello, J. M. Yang, R. Hugo, Y. Lee, and S. S. Park, "Feasibility analysis of blending hydrogen into natural gas networks," *International Journal of Hydrogen Energy*, vol. 48, no. 46, pp. 17605–17629, May 2023.

**Hanchi Zhang** received the B.S. degree and the M.S. degree in Electrical Engineering from North China Electric Power University, Beijing, in 2016 and 2019. He obtained the Ph.D. degree in Energy Technology at the Department of Energy Technology, Aalborg University, Denmark in 2022. He is currently a PostDoc at the Department of Energy Technology, Aalborg University, Denmark. His research focuses on lightning protection, electromagnetic transients and insulation coordination.

**Hongyang Zhou** received the Ph.D. degree in Electrical Engineering from North China Electric Power University (NCEPU), Beijing, China, in 2020. After a Post-Doctoral Fellow with Tsinghua University, Beijing, he is currently working as an Associate Professor with the Xiamen University of Technology, Xiamen, China. His research interests are condition monitoring and optical fiber sensing.

**Filipe Faria da Silva** received the M.Sc. degree in Electrical and Computers Engineering from the Instituto Superior Técnico, Portugal, in 2008, and the Ph.D. degree in electric power systems from Aalborg University, Denmark, in 2011. He was with EDP-Labelec in 2008 and the Danish TSO Energinet from 2008 to 2011. He is currently an Associate Professor with the Department of Energy Technology, Aalborg University, where he is also Semester Coordinator for the Electrical Power System and High Voltage Engineering master program and Leader of the Modern Power Transmission Systems research program. His research focuses on power cables, electromagnetic transients and insulation coordination, power quality, network stability, HVDC transmission, and HV phenomena.

**Claus Leth Bak** received the B.Sc. degree (honors) in Electrical Power Engineering, in 1992, the M.Sc. degree in Electrical Power Engineering in the Department of Energy Technology at Aalborg University, Aalborg, Denmark, in 1994, the Ph.D. degree in 2015 with the thesis "EHV/HV underground cables in the transmission system." After his studies, he worked as a Professional Engineer with Electric Power Transmission and Substations with specializations within the area of Power System Protection at the NV Net Transmission System Operator. In 1999, he was employed as an Assistant Professor at the Department of Energy Technology, Aalborg University, where he holds a Full Professor position today. His main research areas include corona phenomena on overhead lines, composite transmission towers, power system modeling and transient simulations, underground cable transmission, power system harmonics, power system protection, composite materials for EHV power pylons and HVDC-VSC offshore transmission networks. He is chair of the Danish Cigré National Committee, member of CIGRE Technical Council and member of Cigré SC C4 AG1. He received the DPSP 2014 best paper award and the PEDG 2016 best paper award. He received CIGRE Distinguished member award (2020) and CIGRE TC award (2020). He serves as Head of the Energy Technology Ph.D. program and as Head of the Section of Electric Power Systems and Microgrids and is a member of the Ph.D. board at the Faculty of Engineering and Science.